

Far-Infrared Absorption Measurements of Polypeptides and Cytochrome *c* by THz Radiation

Kohji Yamamoto,* Keisuke Tominaga,* Hiroaki Sasakawa,† Atsuo Tamura,*,† Hidetoshi Murakami,†† Hideyuki Ohtake,†† and Nobuhiko Sarukura*,††

Molecular Photoscience Research Center, Kobe University, Nada-ku, Kobe, 657-8501

†Graduate School of Science and Technology, Kobe University, Nada-ku, Kobe, 657-8501

††Institute for Molecular Science, Myodaiji, Okazaki, 444-8585

(Received October 15, 2001)

Pulsed terahertz (THz) radiation and black-body radiation are applied to measure far infrared (FIR) absorption spectra of polypeptides and cytochrome *c* in the wavenumber region from 7 cm^{-1} to 160 cm^{-1}. In the region from 7 cm^{-1} to 55 cm^{-1}, FIR absorption cross sections of polyglycine and poly-L-alanine in powder are greater than those of glycine and L-alanine in powder. On the other hand, FIR absorption spectra of cytochrome *c* in lyophilized powder show little dependence on protein structures. The structures of biopolymers are investigated by mid-IR absorption (polypeptides and cytochrome *c*) and by resonance Raman scattering (cytochrome *c*). FIR spectral features of biopolymers in the THz frequency region are qualitatively discussed in terms of density of states and homogeneous/inhomogeneous broadening.

There has been dramatic progress in techniques of generation and detection of freely propagating terahertz (THz) radiation in this decade.[1–4] Owing to the advance, the THz radiation has been successfully applied to far infrared (FIR) absorption spectroscopy in a broad range of molecular science from gas phases[5,6] to condensed phases.[7–19] The THz frequency region from 1 to 100 cm^{-1} is much lower than frequencies of most internal vibrations of isolated small molecules. In the THz frequency region, spectra in condensed phases contain information on collective motions with a time-scale of picoseconds, which are associated with delocalized and coherent movement of a large number of atoms and molecules. Collective motions are sensitive to perturbation by intermolecular interactions with surrounding molecules as well as changes of intramolecular interactions through structural fluctuations. Therefore, motions in a picosecond time-scale modulate a carrier wave of the THz radiation and can be directly investigated through amplitude- and phase-modulation of the THz radiation.

Structural fluctuations in proteins on a picosecond time-scale have been recently studied in detail by theoretical methods such as molecular dynamics simulation. Significance of THz frequency motions in proteins has been theoretically emphasized through studies of relations between low frequency modes and protein functions.[20–24] The results from the normal mode analysis[25] or the principal component analysis[21] on several proteins indicate the presence of various vibrations in a picosecond time-scale with frequencies down to several wavenumbers. The vibrations have large amplitudes and are globally delocalized. Motions at these frequencies were shown to contribute to a major part of protein fluctuations, which were characterized by mean-square displacements of protein atoms from their vibrational equilibria.[21,22]

THz frequency bands around 20–30 cm^{-1} of proteins were previously observed by Raman scattering[26,27] and inelastic neutron scattering.[28–32] Brown et al.[26] observed a broad band at 29 cm^{-1} in Raman spectra of α-chymotrypsin and considered that this band originated in intramolecular vibrations that involved large portions of atoms. This band was relatively independent of the sample preparation of α-chymotrypsin but was dependent on structures of this protein; the band at 29 cm^{-1} vanished upon SDS denaturation (SDS; sodium dodecyl sulfate). Genzel et al.[27] also reported a Raman band at 25 cm^{-1} of lysozyme. They assigned this band to an intermolecular vibration between proteins because the band was observed in crystalline states but not in solution. In inelastic neutron scattering of lyophilized proteins, a single, broad band centered at about 25 cm^{-1} was frequently observed.[28–30,32] From the experimental observation of this band, Smith[28] concluded that there existed some underdamped vibrations of low frequency modes in proteins.

FIR absorption spectra of polypeptides[33,34] and proteins[35–37] down to the THz frequency region were also measured in the 1970s. Schotts and Sievers[36] reported detailed studies on FIR absorption spectra of polyalanines from room temperature to 4 K. They found that the spectral dependence on temperature was related to the number of residues in alanine-oligomers. FIR transmission spectra of lysozyme at different hydration conditions were measured by using synchrotron radiation, and a band at 19 cm^{-1} was observed.[38] This band was considered to originate in low-frequency vibrations of the protein and/or water molecules perturbed in hydration. Previous studies[33–38] on FIR absorption spectroscopy of biopolymers have mainly dealt with the existence of bands and some qualitative features of these bands. FIR absorption spectra of serum albumin[17] and

DNA[17,19] were recently measured by the THz radiation. Markelz et al.[17] observed that FIR absorption increases by hydration and denaturation, and Brucherseifer et al.[19] observed that transmission and refractive index in the THz frequency region were different between the hybridized state and the denatured state of DNA.

FIR absorption, Raman scattering, and inelastic neutron scattering can be applied to investigate low-frequency motions of biopolymers. However, different nuclear motions contribute to the spectra of the three methods; FIR absorption, Raman scattering, and inelastic neutron scattering originate in dipole-, polarizability-, and density-fluctuations, respectively. Comparison of spectra obtained by these methods is, therefore, important for studies on the low-frequency motions. At the same time, it is essential to investigate relations between structures of biopolymers and spectral features in the low-frequency region. Biopolymers and proteins, whose structures have been studied extensively, should be chosen as samples for that purpose. Polyglycine, poly-L-alanine, and cytochrome *c* are the examples whose structures are well known.

This paper presents FIR absorption spectra of polypeptides and cytochrome *c* measured by using pulsed THz radiation and black-body radiation as light sources. With respect to spectral features, we study FIR absorption dependence on polymerization of amino acids and on protein structures. To investigate the influence of polymerization, we measure FIR absorption spectra of polypeptides (polyglycine and poly-L-alanine) and compare them with those of monomers (glycine and L-alanine). In order to investigate dependence on protein structures, we measure FIR spectra of cytochrome *c* in powder, which are lyophilized from the solutions in the native, the denatured, and the molten globule states. We also compare FIR spectra of cytochrome *c* with those of the polypeptides, whose secondary structures are well verified. Structures of polypeptides and those of cytochrome *c* in powder are determined by vibrational spectroscopy; mid-IR absorption and resonance Raman scattering. Mid-IR absorption (polypeptides and cytochrome *c*) provides information on secondary structures of main chains and on side-chains of carboxy groups, and resonance Raman scattering (cytochrome *c*) provides information on tertiary structures around the heme and on heme states.

Experimental Procedures

Apparatus of FIR Absorption Measurements. The configuration of our FIR absorption spectrometer (7 – 55 cm^{-1}) is depicted schematically in Fig. 1; it consists of a generation system and a detection system of the THz radiation. A mode-locked Ti : sapphire laser (Mai Tai, Spectra-Physics) is used to pump a non-doped bulk InAs semiconductor. Pulses at 800 nm with a 70-fs width are provided, with an energy of 11 nJ at an 80-MHz repetition rate (900 mW at average power). The THz radiation is generated by weakly focusing the femtosecond pulse to 2 mm in diameter on a (100)-surface of the InAs semiconductor wafer. The THz radiation is considered to generate through electric dipole radiation; carriers which are photogenerated on the surface of the semiconductor are accelerated by a built-in depletion electric field.[1,2,39] To enhance the intensity of the THz radiation, the semiconductor is placed in a magnetic flux density of 1.7 T so that its (100)-surface is parallel to the direction of the magnetic flux density and so that the incident angle for the pump laser is about 70 degree to the surface normal.[40] It was reported that two orders of magnitude increase of the THz radiation in power was obtained from the InAs surface by adding a magnetic flux density of 2 T.[3,4] Power spectra of the THz radiation are measured by a polarizing Michelson interferometer (Graseby Specac). The intensity of the THz radiation is detected by a liquid-helium-cooled Ge bolometer (QGEB/2F, QMC Instruments) with a lock-in amplifier (SR-830, Stanford Research Systems) operating at 200 Hz. The system in Fig. 1 is open to air except for the inside of the vacuum-sealed interferometer. When measuring FIR absorption from 55 cm^{-1} to 160 cm^{-1}, the radiation from a black-body at 1000°C (IR-563, Graseby Infrared) is used as a light source. The FIR absorption system using the black-body radiation is the same as that illustrated in Fig. 1, except for a replacement of the THz-generation part with the black-body. Spectral resolutions of all the measured FIR spectra are 0.5 cm^{-1} and 1.3 cm^{-1} when using the THz radiation and the black-body radiation, respectively.

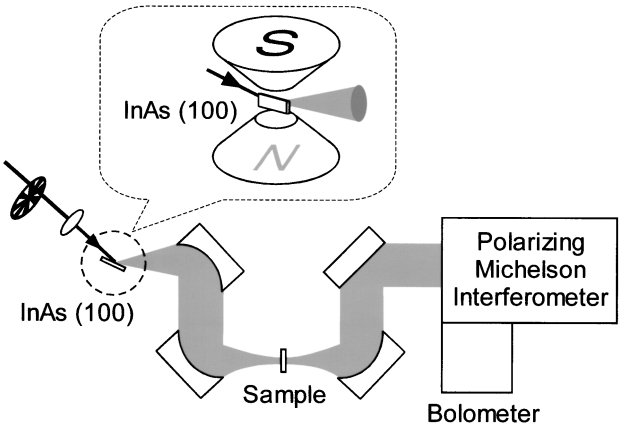

Fig. 1. FIR absorption spectrometer using the THz radiation. Pulses at 800 nm with 70-fs width at 80-MHz repetition rate irradiate an InAs wafer, which is placed in a magnetic flux density of 1.7 T generated by an electromagnet. The (100)-InAs surface is parallel to a direction of the magnetic flux density. The THz radiation from the (100)-InAs is collimated by an off-axes parabolic mirror. The THz radiation is focused at a sample position and collimated again by an off-axes mirror. Intensity of the THz radiation is detected by a germanium bolometer which is cooled by helium liquid. Chopping frequency of the pump pulse is 200 Hz. A polarizing Michelson interferometer is vacuum-sealed. All the FIR absorption system other than the polarizing Michelson interferometer is open to air. When using the black-body radiation for FIR absorption measurements, the generation part of the THz-radiation is replaced by a black-body.

Calculation of FIR Absorption Spectra. Figure 2 shows power spectra of light sources; (A) THz radiation and (B) black-body radiation. Sharp dip lines observed in Figs. 2(A) and 2(B) are absorption lines of water vapor. Figure 2(A) ensures that the frequency region from 7 cm^{-1} to 55 cm^{-1} can be available for measuring FIR absorption by the THz radiation. The low frequency limit of 7 cm^{-1} is determined by a beam-splitter inside the interferometer. When the black-body radiation is used, the frequency region from 15 cm^{-1} to 160 cm^{-1} is measurable, as shown in Fig. 2(B). The frequency regions available by the THz-radiation

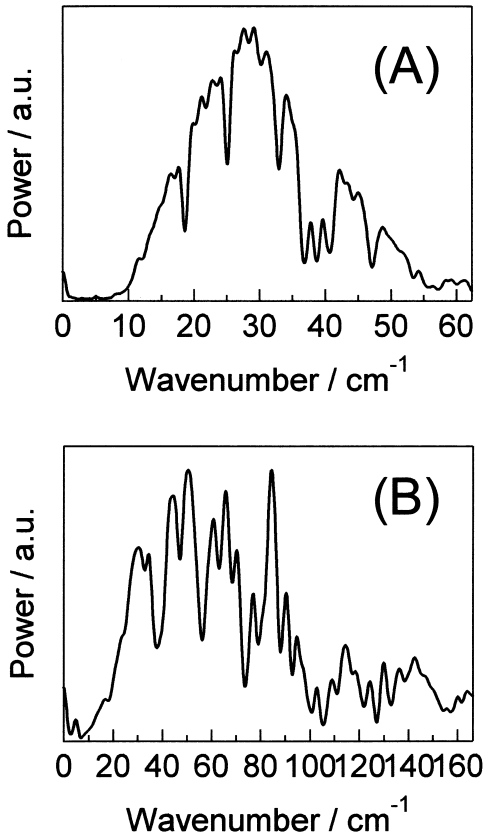

Fig. 2. Power spectra of light sources; (A) THz radiation and (B) black-body radiation. The ordinate scales in (A) and (B) are arbitrary. Resolutions of (A) and (B) are 0.5 cm^{-1} and 1.3 cm^{-1}, respectively.

and the black-body radiation are overlapped from 15 cm^{-1} to 55 cm^{-1}.

FIR absorption spectra are determined from the power spectra of transmitted radiation. An FIR absorption spectrum is represented by the absorption cross section, $\sigma(\tilde{\nu})$, in units of m^2/mol. This is calculated by

$$\sigma(\tilde{\nu}) = -\frac{V}{N}\ln\left(\frac{I(\tilde{\nu})}{I_0(\tilde{\nu})}\right). \quad (1)$$

Here, $I(\tilde{\nu})$ and $I_0(\tilde{\nu})$ are the power spectra of the radiation with and without the sample at the wavenumber $\tilde{\nu}$, respectively. V is the volume of the sample in units of m^3 and N is the mole number of the sample.

Sample Preparation and Spectral Measurements. Samples of polypeptides and amino acids are commercially available powders: polyglycine (P-0254, Sigma), poly-L-alanine (Miles-Yeda), glycine and L-alanine (Wako). These samples are used without any purification. Protein samples in powder are prepared by lyophilizing aqueous (H_2O) solutions of cytochrome *c* (Wako) in the native, the pH-denatured, and the molten globule states. No buffer is added in the initial solution of the native state. The initial solution of the denatured state is adjusted at pH = 2.0 by hydrochloric acid. That of the molten globule state contains 0.1 M (1 M = 1 mol dm^{-3}) potassium chloride and its pH is adjusted to 2.4 by hydrochloric acid.[41]

The samples in powder are pressed to self-standing pellets with 3 mm or 5 mm in diameter for FIR absorption measurements. Typical thicknesses of pellets of the polypeptides and cytochrome *c* are 250 μm when using the THz radiation and 60 μm when using the black-body radiation. It is essential to change the thickness of the samples when measuring FIR absorption spectra in different frequency regions. There are two reasons for it. One is to increase absorption because FIR absorption below 55 cm^{-1} is much weaker than the one over 55 cm^{-1}. The other is to reduce fringes appearing in the FIR spectra. The fringe effect or the etalon effect arises from multiple reflections inside the sample and appears noticeably when a half of the wavelength is equal to a sample thickness. For example, in a case that 50-cm^{-1} radiation transmits through a sample whose refractive index is 2, the fringe effect stands out when the sample thickness is 50 μm. FIR absorption spectra in the overlapping frequency region from 15 cm^{-1} to 55 cm^{-1} obtained by the THz radiation and by the black-body radiation ought to agree with each other with respect to the quantity of the absorption cross section. In practice, however, those obtained by the black-body radiation are upper-shifted by a constant value in comparison with those obtained by the THz radiation. This vertical shift may occur due to reflection and/or lens effect when transmitting through the samples. When the sample is thin, small changes in the intensity of transmitted light due to these effects exert much influence on determination of the absorption cross section. To reduce these effects appearing in FIR absorption cross sections, an FIR absorption spectrum measured by the black-body radiation is shifted by a constant value to the one measured by the THz radiation to attain a best overlap between these two spectra from 15 cm^{-1} to 55 cm^{-1}. All the FIR absorption spectra from 7 cm^{-1} to 160 cm^{-1} shown in this paper are obtained by this procedure. FIR absorption spectra per one sample are measured more than 15 times in total by changing the thickness of the samples (30 – 300 μm for the polypeptides and cytochrome *c*, and 30–1000 μm for the amino acids). As for polypeptides and cytochrome *c*, vertical offsets are several percentages with respect to the peak values of the FIR absorption bands around 100 cm^{-1}: 3% for polyglycine, 5% for poly-L-alanine, 4% for cytochrome *c* in the native state, and 2% for cytochrome *c* in the denatured state. As for monomers (glycine and L-alanine) the offsets are obtained in a similar way. All the FIR spectra are measured at room temperature, 25°C.

Mid-IR absorption spectra of the polypeptides in powder and those of cytochrome *c* in lyophilized powder are measured by an FT-IR spectrometer (Spectrum 1000, Perkin Elmer). Samples are dispersed by KBr powder and are pressed to self-standing pellets. Optical densities of pellets are adjusted to about 1, and resolution of all the mid-IR spectra is 1 cm^{-1}. Resonance Raman spectra of cytochrome *c* are measured upon Soret-band excitation by 413.1-nm light delivered from a cw Kr^+-laser (Model 2060, Spectra-Physics). Samples of cytochrome *c* in solution and in lyophilized powder are set in a spinning cell when measuring resonance Raman spectra in order to avoid continuous irradiation of the same portion of the samples. Lyophilized powders of cytochrome *c* in the spinning cell are in the form of pressed-pellets. The scattered light at 90°-angle is collected and dispersed by a 25-cm single imaging spectrograph (250IS, Chromex). To remove the excitation light, a holographic notch filter is placed between the sample and an entrance slit of the spectrograph. The dispersed light is detected with a charge coupled device (CCD) (CCD3200, Astromed).

Results and Discussion

Polypeptides. Conformations of Polypeptides in Powder. Secondary structures of polypeptides in powder are investigated by mid-IR absorption. Figure 3 represents mid-IR absorption spectra of the polypeptides in powder: (a) polyglycine and (b) poly-L-alanine. The relation between structures of polypeptides and mid-IR absorption spectra was studied[42,43] in detail. Polyglycines have two possible structures, called polyglycine I and polyglycine II. Polyglycine I has the β-structure of the antiparallel-chain rippled sheet, and polyglycine II has the 3_1-helix of the threefold helical chains. Figure 3(a) coincides with the reported mid-IR spectrum[42,43] of polyglycine I except for the amide I band around 1650 cm^{-1}. The amide I band in Fig. 3(a) is split, whereas the one in the reported spectrum is broad with a shoulder at the high frequency side. The apparent difference in the amide I band may occur from the lower resolution of the reported spectrum or from some difference of sample preparation. Figure 3(a), however, definitely differs from the spectrum of polyglycine II in the entire mid-IR region.[42,43] We, therefore, conclude that the polyglycine sample we use has the β-structure of polyglycine I. Poly-L-alanines also have two possible structures, called α-poly-L-alanine and β-poly-L-alanine. The structure of α-poly-L-alanine is the α-helix, and that of β-poly-L-alanine is the antiparallel-chain pleated sheet. Figure 3(b) agrees with the mid-IR absorption spectrum of α-poly-L-alanine, but not with that of β-poly-L-alanine.[42,43] Both parallel and perpendicular polarization components of IR absorption are observed in Fig. 3(b) because the sample is randomly oriented. The amide I band at 1658 cm^{-1}, the amide II band at 1545 cm^{-1}, and the amide-III band at 1272 cm^{-1} are, in particular, characteristic frequencies of α-poly-L-alanine. The poly-L-alanine we use, therefore, has the α-helical structure.

FIR Absorption Spectra of Polypeptides and Monomers. We represent FIR absorption spectra of polypeptides and their monomers, and describe their spectral features in this subsection. Figure 4 shows the FIR absorption spectra of polyglycine I (solid line) and glycine (dotted line). The absorption cross section of polyglycine I is calculated according to Eq. 1 with N equal to the total mole number of glycine residues in the sample. The solid line in Figure 4, therefore, represents the average absorption cross section of one mole of glycine residue. This quantity is comparable with the absorption cross section per one mole of glycine in the dotted line in Fig. 4.

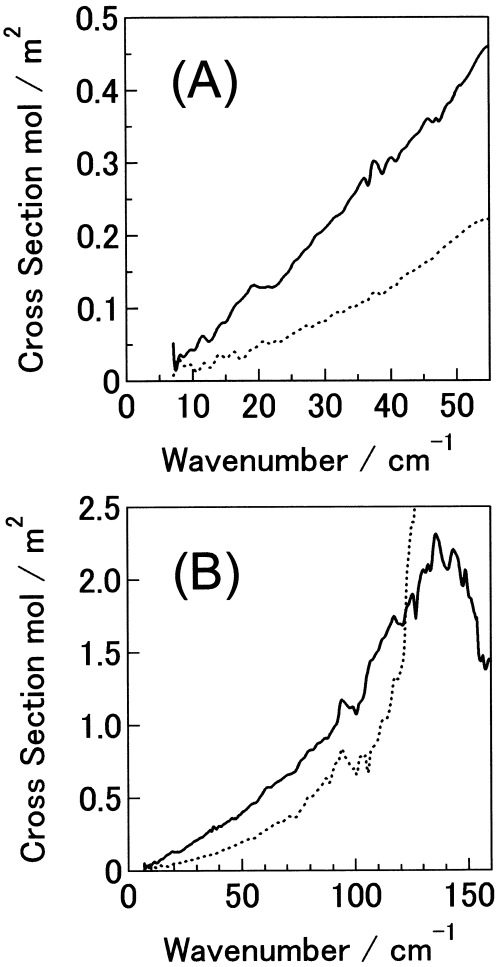

Fig. 4. FIR absorption spectra of polyglycine I and glycine; (A) is an enlarged figure of (B) below 55 cm^{-1}. Solid lines represent average absorption cross section of polyglycine I per one mole of glycine residues and dotted lines represent absorption cross section of one mole of glycine. Both samples are pressed pellets without any dispersing powders.

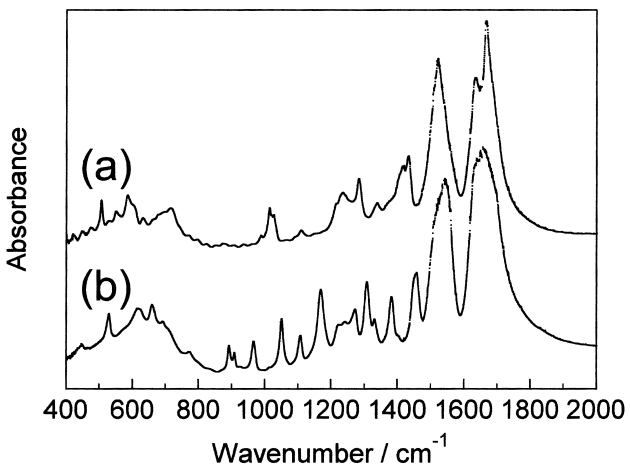

Fig. 3. Mid-IR absorption spectra of polypeptides; (a) polyglycine and (b) poly-L-alanine. Polypeptide samples are dispersed by KBr and are pressed to pellets.

Interesting features are observed in the FIR absorption intensity and band appearances in Fig. 4. First, in Fig. 4(A), the FIR absorption cross section in the THz frequency region increases by more than twice upon polymerization of glycine. Second, no band of polyglycine I in the THz frequency region is observed in Fig. 4(A), though an IR-active band at 37 cm^{-1} was predicted by the normal mode analysis of polyglycine I with the β-structure of the antiparallel-chain rippled sheet.[42,43] Normal modes were calculated on the assumption that this β-structure has C_{2h} symmetry in a unit cell. According to this calculation, the band at 37 cm^{-1} arise mainly from NH···O and

CO···H in-plane angle bends. IR-active bands at 108 cm^{-1} and at 140 cm^{-1} were also predicted in polyglycine I.[42,43] The band at 140 cm^{-1} is explicitly observed in Fig. 4(B). This mode originates in combination of the H···O stretch between anti-parallel chains, C–N twist and N–H out-of-plane angle bend.[42,43] The other predicted mode has large contributions of skeletal deformation and skeletal torsion,[42,43] but it is difficult to judge if a band at 108 cm^{-1} exists or not in Fig. 4(B).

The same features are observed in the FIR absorption spectra of α-poly-L-alanine and L-alanine. Figure 5 represents the FIR absorption cross section of α-poly-L-alanine (solid line) and that of L-alanine (dotted line). The ordinates of the solid line and the dotted line are the absorption cross sections per one mole of alanine residues and per one mole of alanine, respectively. Upon polymerization of L-alanines, the FIR absorption cross section in the THz frequency region increases by more than three times in Fig. 5(A). An explicit band at 120 cm^{-1} and a shoulder at 85 cm^{-1} are recognized in Fig. 5(B).

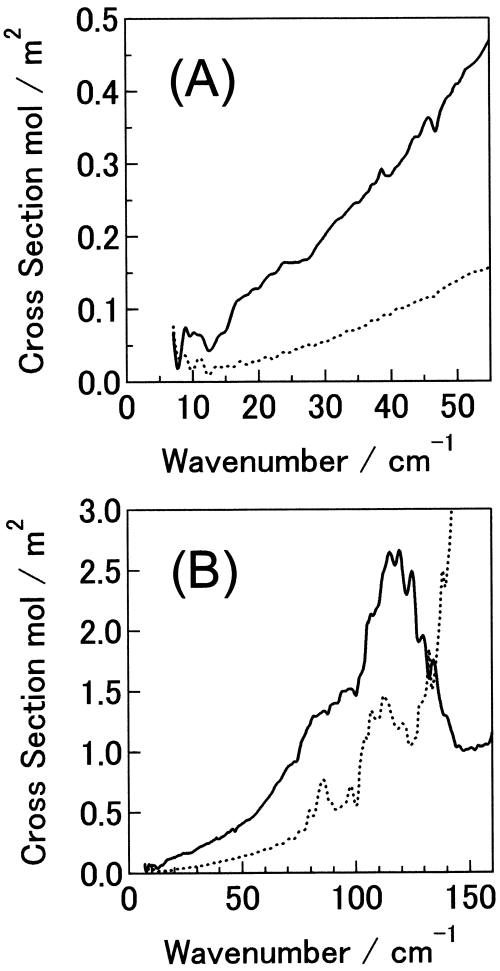

Fig. 5. FIR absorption spectra of α-poly-L-alanine and L-alanine; (A) is an enlarged figure of (B) below 55 cm^{-1}. Solid lines represent average absorption cross section of α-poly-L-alanine per one mole of L-alanine residues and dotted lines represent absorption cross section of one mole of L-alanine. Both samples are pressed pellets without any dispersing powders.

These observed bands are in accord with the IR-active bands at 85 cm^{-1} and 120 cm^{-1} predicted by the normal mode analysis of α-poly-L-alanine with the α-helical structure,[42–44] which were calculated on the assumption of the right-handed α-helix with 47 residues in 13 turns as a unit cell. These vibrations at 85 cm^{-1} and 120 cm^{-1} are associated with skeletal deformation and skeletal torsion, respectively. Another band at 40 cm^{-1} (originating in NH out-of-plane angle bend and $-C^{\beta}H_3$ bend) was also predicted, but no explicit band in the THz frequency region is observed in Fig. 5(A). A band at 40 cm^{-1} was also absent in the previously reported FIR absorption spectra of poly-L-alanine.[34,36]

Cytochrome *c*. Conformation of Cytochrome *c* in Lyophilized Powder. Tertiary structures around the heme and the heme states of cytochrome *c* in lyophilized powder are first examined by resonance Raman scattering. Later, their secondary structures and protonation states of carboxy groups are investigated by mid-IR absorption.

Figure 6 shows resonance Raman spectra of cytochrome *c* in different conditions and states as follows: (a) the lyophilized powder from the solution in the denatured state with pH = 2,

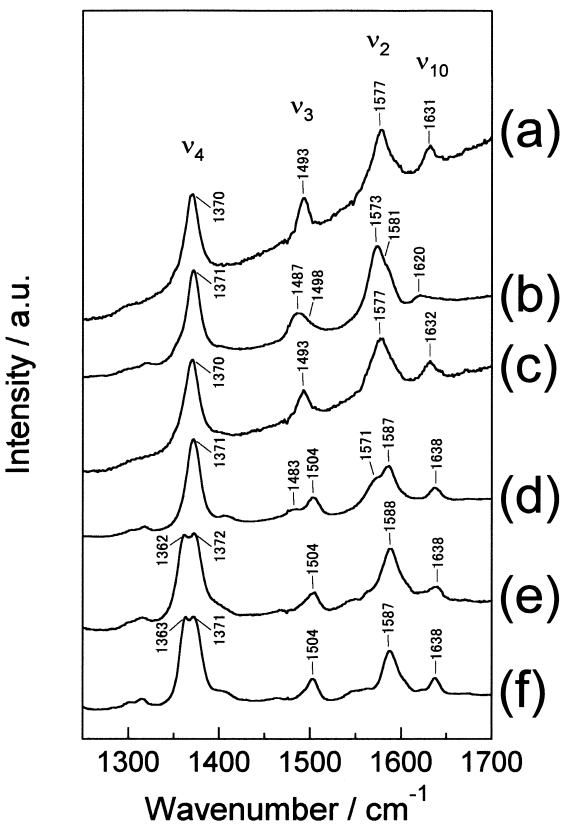

Fig. 6. Resonance Raman spectra of cytochrome *c* by 413.1-nm excitation; (a) the lyophilized powder from the solution in the pH-denatured state at pH = 2.0, (b) the solution in the pH-denatured state at pH = 2.0, (c) the lyophilized powder from the solution in the molten globule state at pH = 2.4 with 0.1-M KCl, and (d) the solution in the molten globule state at pH = 2.4 with 0.1-M KCl, (e) the lyophilized powder from the solution in the native state, and (f) the solution in the native state.

(b) the solution in the denatured state with pH = 2, (c) the lyophilized powder from the solution in the molten globule state at pH = 2.4 with 0.1-M KCl, (d) the solution in the molten globule state at pH = 2.4 with 0.1-M KCl, (e) the lyophilized powder from the solution in the native state, and (f) the solution in the native state without any buffer. Resonance Raman spectra of heme proteins by Soret-band excitation reflect environmental structures around the heme inside the protein as well as heme conformations.[45–50] Information on tertiary structures of cytochrome *c* can, therefore, be obtained through resonance Raman spectra. Frequencies of the ν_2 band, the ν_3 band, and the ν_{10} band are, in particular, correlated to the core size of the heme,[45] which is dependent on the spin-state and the coordination state of the heme.

The resonance Raman spectra of cytochrome *c* in solution are discussed here. The ν_2 band at 1587 cm^{-1}, the ν_3 band at 1504 cm^{-1} and the ν_{10} band at 1638 cm^{-1} in Fig. 6(f) shows that cytochrome *c* in the native state in solution is in the six-coordinated low-spin state, but the ν_4 band at 1363 cm^{-1} and 1371 cm^{-1} indicates that it is in ferric and ferrous mixture. Figure 6(b) shows the ν_2 band at 1573 cm^{-1} and the ν_3 band at 1487 cm^{-1}, which are characteristic for the six-coordinated high-spin state. It also shows the bands of the species in the five-coordinated high-spin state; the ν_{10} band at 1620 cm^{-1}, the ν_2 band with a shoulder at 1581 cm^{-1}, and the broad ν_3 band with high frequency side at around 1498 cm^{-1}. Figure 6(d) shows the ν_2 band at 1587 cm^{-1} and 1571 cm^{-1}, the ν_3 band at 1504 cm^{-1} and 1483 cm^{-1}, and the ν_{10} band at 1638 cm^{-1}. These indicate that the solution in the molten globule state contains the six-coordinated low-spin state and the six-coordinated high-spin state.

The resonance Raman spectra in lyophilized powder are compared with those in solution. With respect to the native state, Fig. 6(e) agrees very well with Fig. 6(f). Cytochrome *c* in lyophilized powder from the solution in the native state, therefore, preserves the tertiary structure around heme in the native state in solution. On the other hand, Figs. 6(a) and 6(c) are different from Figs. 6(b) and 6(d), respectively. The tertiary structures in the pH-denatured and the molten globule states in solution are changed by lyophilization. Figures 6(a) and 6(c), however, have the same frequencies of the resonance Raman bands; the ν_2 band at 1577 cm^{-1}, the ν_3 band at 1493 cm^{-1}, and the ν_{10} band at 1631 cm^{-1}. These observed bands indicate that cytochrome *c* in lyophilized powder from the solutions in the pH-denatured state have the same structure as that in lyophilized powder from the solutions in the molten globule state.

Figure 7 represents mid-IR absorption spectra of cytochrome *c* in lyophilized powder, (a) the lyophilized powder from the solution in pH-denatured state, (b) the lyophilized powder from the solution in the molten globule state, and (c) the lyophilized powder from the solution in the native state. Figures 7(a) and 7(b) agree with each other. This indicates that the lyophilized powders from the solutions of the pH-denatured and molten globule states are equivalent in terms of the secondary structures. Figure 7(c) is, however, different from Fig. 7(a) and 7(b). Figure 7(d) is a difference spectrum: that is Fig. 7(a) minus Fig. 7(c). The ordinate scale of Fig. 7(d) displayed is multiplied by two. Intensity decreases in the amide I band at 1655 cm^{-1} and in the amide Ⅲ band at 1314 cm^{-1} can

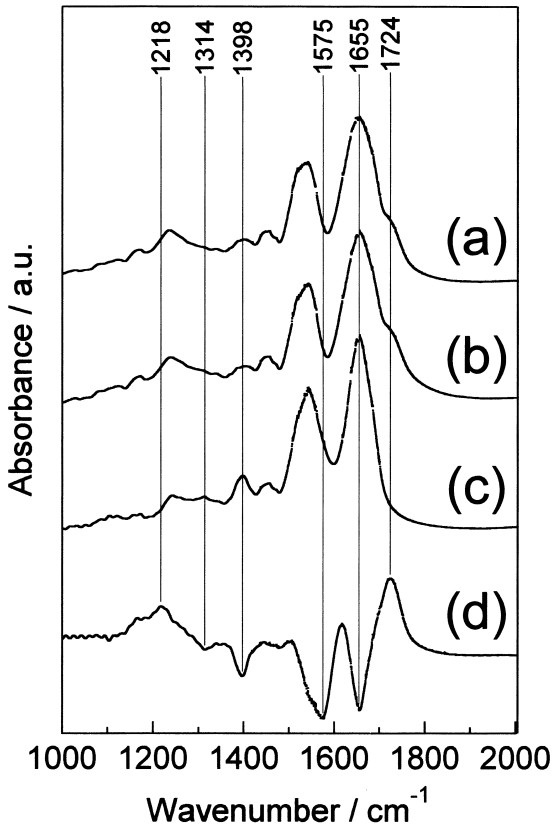

Fig. 7. Mid-IR absorption spectra of cytochrome *c* in lyophilized powder; (a) lyophilized powder from the solution in the pH-denatured state at pH = 2.0, (b) lyophilized powder from the solution in the molten globule state at pH = 2.4 with 0.1-M KCl, (c) lyophilized powder from the solution in the native state, and (d) difference spectrum equal to 2×[(a)−(c)]. Samples in lyophilized powder are dispersed by KBr and are pressed to pellets.

be recognized in Fig. 7(d). These decreases indicate[51–53] that the α-helical content in Fig. 7(a) decreases in comparison with that in Fig. 7(c). An intensity increase in the amide Ⅲ region from 1190 cm^{-1} to 1285 cm^{-1} is also observed in Fig. 7(d). The increase of this broad band indicates that amounts of random structure and probable other structures such as β-structure increase in Fig. 7(a).[52,54] The secondary structure of the lyophilized powder of cytochrome *c* from the solution of the pH-denatured state is, therefore, different from that from the solution in the native state.

The bands at 1398, 1575, and 1724 cm^{-1} are also observed in Fig. 7(d). These bands can be assigned to carboxy groups in side-chains of glutamic acids and aspartic acids. Cytochrome *c* has 9 residues of glutamic acids and 3 residues of aspartic acids. The band at 1724 cm^{-1} is assigned to the C=O stretch of protonated carboxy groups (–COOH) and the bands at 1398 and 1575 cm^{-1} are symmetric and asymmetric stretches, respectively, of deprotonated carboxy groups ($-COO^-$).[54–56] Intensity increase of 1724-cm^{-1} band and intensity decrease of 1398- and 1575-cm^{-1} bands in Fig. 7(a) suggest that the lyophilized powder of cytochrome *c* from the solution of the pH-denatured state maintains the denatured condition in the solu-

tion of pH = 2 with respect to the carboxy side-chains. Spectral changes in the mid-IR region similar to those in Fig. 7 have been observed[51] in guanidine-hydrochloride denaturation of iso-1-cytochrome *c* in H_2O solution at pH = 7.5, except for the band changes of the carboxy groups at 1398, 1575, and 1724 cm^{-1}. They may not be observed in Ref. 51 because side-chains of glutamic acids and aspartic acids are not protonated at pH = 7.5.

In summary, the lyophilized powder of cytochrome *c* from the solution in the native states has the same conformation as that in the native state in solution. The lyophilized powders of cytochrome *c* from the solution in the pH-denatured and the molten globule states has the same conformation in terms of the secondary and tertiary structures. Their conformations are, however, different from that of the lyophilized powder from the solution in the native state. They are also different from the conformations of cytochrome *c* in the pH-denatured and molten globule states in solution.

FIR Absorption Spectra of Cytochrome *c*. Figure 8 displays FIR absorption spectra of cytochrome *c* in lyophilized powder. The solid and dotted lines depict absorption cross sections per one mole of cytochrome *c* in the native state and in the pH-denatured state, respectively. An FIR spectrum in lyophilized powder from the solution of the molten globule state is not shown because of the conformational similarity between cytochrome c in lyophilized powder from the solutions of the pH-denatured and the molten globule state. It is recognized that the two FIR spectra in Fig. 8 resemble each other very well up to 160 cm^{-1}. Structures of cytochrome *c*, however, are different from each other in terms of secondary and tertiary structure, as shown in Figs. 6 and 7. This result shows that FIR absorption spectra of cytochrome *c* in lyophilized powder at room temperature are not dependent on secondary and tertiary structures. Another feature is that FIR absorption spectra of cytochrome *c* in the native and in the denatured states have profiles of monotonic increase up to 130 cm^{-1}, and that no band is observed around 20 cm^{-1}. The monotonic and featureless profiles in the THz frequency region are similar to those of polypeptides from 7 cm^{-1} to 70 cm^{-1}. This observation is in contrast with a previously reported IR-band at 19 cm^{-1} of lysozyme[38] and with the boson peaks which are frequently observed in neutron scattering.[28–32] No explicit band is observed from 80 cm^{-1} to 160 cm^{-1} in Fig. 8(B). The band absence in this region of cytochrome *c* is in remarkable contrast with FIR absorption spectra of polypeptides in Figs. 4(B) and 5(B).

FIR Absorption Profiles. FIR Absorption Intensity Dependent on Polymerization. An absorption cross section $\sigma(\tilde{\nu})$ is related to a total dipole moment of a sample, $\boldsymbol{M}(t)$, through the following equations:[57–59]

$$\sigma(\tilde{\nu}) = \frac{4\pi^3 N_A}{3\varepsilon_0 hn(\tilde{\nu})}\tilde{\nu}\left(1-e^{-\beta hc\tilde{\nu}}\right)I_{MM}(\tilde{\nu}) \quad (2)$$

$$I_{MM}(\tilde{\nu}) = \frac{1}{2\pi N}\int_{-\infty}^{\infty} dt e^{-i2\pi c\tilde{\nu}t}\langle \boldsymbol{M}(0)\cdot\boldsymbol{M}(t)\rangle \quad (3)$$

$$\boldsymbol{M}(t) = \sum_{j=1}^{N}\boldsymbol{\mu}_j(t) \quad (4)$$

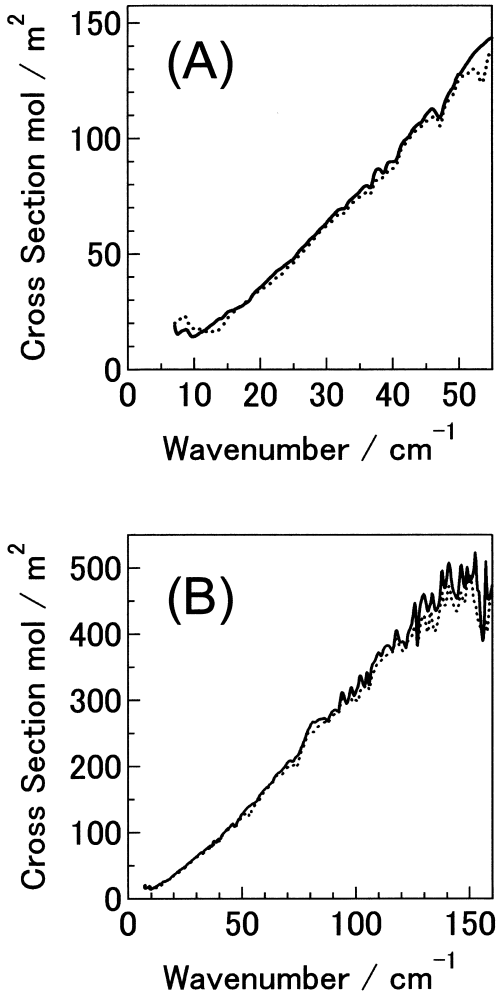

Fig. 8. FIR absorption spectra of cytochrome *c* in lyophilized powder; (A) is an enlarged figure of (B) below 55 cm^{-1}. Solid lines and dotted lines represent absorption cross sections of cytochrome *c* in the native and pH-denatured states, respectively.

$I_{MM}(\tilde{\nu})$ is the lineshape function defined as Fourier transform of the time-correlation function of the total dipole moment, divided by *N* (the number of molecules in the sample). The lineshape function is represented as the normalized quantity per one molecule. $\boldsymbol{\mu}_j(t)$ is the individual dipole moment of one molecule, which includes induced dipole moment. N_A is the Avogadro constant, ε_0 the dielectric constant in vacuum, *c* the speed of light, *h* the Planck constant, $n(\tilde{\nu})$ the refractive index of a sample, and $\beta = 1/k_BT$ where k_B and *T* are the Boltzmann constant and the temperature, respectively. The absorption cross section is, therefore, proportional to the product of the lineshape function, $I_{MM}(\tilde{\nu})$, and the frequency factor dependent on temperature, $\tilde{\nu}(1-e^{-\beta hc\tilde{\nu}})$. In Figs. 4(A) and 5(A), absorption cross sections of polyglycine I and α-poly-L-alanine, which are averaged per one residue, are larger than those of the respective monomers. This result means that polymerization enhances frequency components lower than 55 cm^{-1} in the lineshape function.

If a sample is assumed to consist of harmonic oscillators which are not coupled with each other, the absorption cross

section is written in the following expression:[60,61]

$$\sigma(\tilde{\nu}) \propto \left|\left(\frac{\partial \boldsymbol{M}}{\partial q}\right)_0\right|_{\tilde{\nu}}^2 \frac{Z(\tilde{\nu})}{N} \tag{5}$$

$\left(\frac{\partial \boldsymbol{M}}{\partial q}\right)_0$ is the first derivative of the total dipole moment around equilibrium geometry and $\{q\}$ is the normal coordinates of the sample. $Z(\tilde{\nu})$ is the density of states of samples, and $\frac{Z(\tilde{\nu})}{N}$ represents the normalized density of states per one molecule. Charge distribution of a monomer in the electronic ground state changes by polymerization. It is considered that polarization of one residue in polymer is larger than that of amino acid monomer. This effect makes the first derivative of the total dipole moment of the sample increase by polymerization. The increase of polarization also shifts frequencies of normal vibrations to lower values. Motions in the THz frequency region reflect collective motions of samples, and the normalized density of states in the THz frequency region would increase by polymerization. Both the first derivative of the total dipole moment and the normalized density of states are, therefore, inclined to increase of the FIR absorption cross section upon polymerization. The increase of the absorption cross section in the low frequency region upon polymerization reflects characteristics of collective motions in biopolymers. At this point, however, we can not differentiate contributions of these two factors in the FIR absorption increase shown in Figs. 4(A) and 5(B).

Comparison of FIR-Absorption Profiles Dependent on Constituents and Structures. We discuss influences of inhomogeneous broadening upon the FIR absorption spectral features at first and consider the possible necessity of homogeneous broadening later.

IR-active bands around 40 cm^{-1} were predicted in the FIR absorption spectra of polyglycine I and α-poly-L-alanine, but no explicit bands are observed in our measurements. One possible cause for this discrepancy may be due to some decrease of symmetry in the samples. In the normal mode calculation,[42–44] the polypeptides were assumed to have symmetries of periodicity like a crystal. However, the samples of polypeptides we used are not in a crystal. It was also suggested that the crystalline content of poly-L-alanine decreases by polymerization.[36] In contrast to no observation of the IR bands around 40 cm^{-1}, the band at 140 cm^{-1} in polyglycine I and the bands at 120 cm^{-1} and 85 cm^{-1} in α-poly-L-alanine are observed as predicted by the normal mode calculation. According to this calculation,[42–44] the modes of these bands contain large portions of skeletal deformation and torsion. The modes around 40 cm^{-1} have little contributions of skeletal motions, but those of motions related to hydrogen bonds and side-chains. It is, therefore, suggested that the predicted modes around 40 cm^{-1} are easily perturbed by small changes of chain conditions and that the bands are inhomogeneously broadened to a great extent.

The FIR absorption spectra of cytochrome *c* in Fig. 8(B) show broad and featureless profiles from 7 cm^{-1} to 160 cm^{-1}. Cytochrome *c* in the native state is a globular protein which has five α-helices with no β-structures[62] (PDB Code: 1HRC). From the fact that these five α-helices contain 47 residues[62] and that the FIR absorption cross section at 120 cm^{-1} is 2.6 m^2 per 1-mole alanine residue in Fig. 5(B), the absorption cross section of a band at 120 cm^{-1} originating in the α-helices is estimated to be 110 m^2 per 1-mole cytochrome *c*. According to this simple estimation, a band at 120 cm^{-1} should be observed in Fig. 8(B). The bands at 85 cm^{-1} and 120 cm^{-1} of α-poly-L-alanine are considered to originate in backbone vibrations of the α-helical structure.[42,43] The featureless absorption profile in Fig. 8(B) can be qualitatively accounted for by two effects: one is that α-helices in cytochrome *c* are shorter than those of α-poly-L-alanine; three α-helices of cytochrome *c* are shorter than 2 turns, and the other two contain 3 to 4 turns.[62] The second effect is due to the different constituents of amino acids between cytochrome *c* and α-poly-L-alanine; cytochrome c is a heteropolypeptide, and α-poly-L-alanine is a homopolypeptide. This also makes nonperiodic intramoleclar interactions such as hydrogen bonds, electrostatic interaction, van der Waals force, hydrophobic and hydrophilic interaction. These two effects inhomogeneously broaden the FIR absorption bands originating in backbone vibrations. These two effects, however, can not sufficiently explain the agreement of the FIR absorption spectra of cytochrome *c* in the native and the denatured states because these protein samples have definitely different structures.

We consider the influences of homogeneous broadening upon the spectral features. Other causes for the monotonic behaviors in the spectra of polypeptides and cytochrome *c* below 50 cm^{-1} may be due to fast decay of correlation function of the total dipole moment or effects of homogeneous broadening. To examine the homogeneous broadening effect, we consider a simple model of an IR absorption profile of a single oscillator. The dipole correlation function of one mode behaves as a damped oscillation, expressed in the following;

$$\langle \boldsymbol{M}(0) \cdot \boldsymbol{M}(t) \rangle = \frac{1}{3} \langle M^2 \rangle e^{-\frac{|t|}{\tau}} \cos(2\pi c \tilde{\nu}_0 t) \tag{6}$$

where τ is the relaxation time, and $\tilde{\nu}_0$ is the wavenumber of this oscillator. The absorption cross section can be calculated according to Eqs. 2 and 3. Figure 9 represents absorption cross sections against the scaled wavenumber, $\tilde{\nu}' = \frac{\tilde{\nu}}{\tilde{\nu}_0}$, with $\tau = 0.2$ ps and $T = 25$°C; (A) $\tilde{\nu}_0 = 33$ cm^{-1}, (B) $\tilde{\nu}_0 = 120$ cm^{-1}, and (C) $\tilde{\nu}_0 = 1600$ cm^{-1}. Figure 9 exemplifies the effect of homogeneous broadening; the absorption band in the low frequency region is broadened and quite distorted when the relaxation time is in the order of subpicoseconds. Therefore, homogeneous broadening with fast relaxation as well as inhomogeneous broadening are considered to bury bands around 40 cm^{-1} in the polypeptides and to make the FIR absorption spectra of cytochrome *c* from 7 cm^{-1} to 160 cm^{-1} independent of the structures.

Summary

FIR absorption spectra of polypeptides and cytochrome *c* in the wavenumber region from 7 cm^{-1} to 160 cm^{-1} are measured by the THz radiation and the black-body radiation as light sources. FIR absorption cross sections of the polypeptides in the region from 7 cm^{-1} to 55 cm^{-1} are enhanced upon polymerization. This enhancement is considered to originate in the increase of polarization and low-frequency-shift of density of

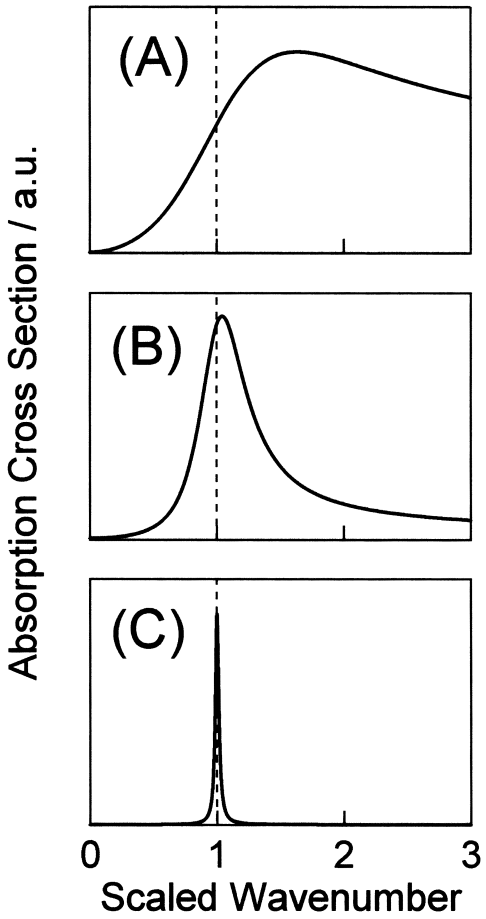

Fig. 9. Absorption cross section originating in a damped oscillator with $\tau = 0.2$ ps and $T = 25$°C; (A) $\tilde{\nu}_0 = 33$ cm^{-1}, (B) $\tilde{\nu}_0 = 120$ cm^{-1}, and (C) $\tilde{\nu}_0 = 1600$ cm^{-1}. The abscissa is the scaled wavenumber.

states upon polymerization. FIR absorption spectra of the polypeptides and cytochrome *c* present no FIR bands around 40 cm^{-1}. Those of cytochrome *c* also show featureless profiles up to 160 cm^{-1}, which are independent of the protein structures. FIR absorption features of biopolymers are qualitatively interpreted by homogeneous broadening due to dynamics with fast relaxation and by inhomogeneous broadening due to decrease in symmetry, short extension of secondary structures, and different constituents of amino acids.

The conformations of biopolymer samples in powder or in lyophilized powder are identified by mid-IR absorption (polypeptides and cytochrome *c*) and by resonance Raman scattering (cytochrome *c*) in the following: (1) The secondary structures of polyglycine and poly-L-alanine used have the antiparallel-chain rippled sheet (polyglycine I) and the α-helical structures (α-poly-L-alanine), respectively. (2) The lyophilized powder of cytochrome *c* from the solution in the native state has the same conformation as that in the native state in solution. (3) The lyophilized powders of cytochrome *c* from the solution in the pH-denatured and the molten globule states have the same conformation in terms of the secondary and tertiary structures, although its conformation is different from that of the lyophilized powder obtained from the solution in the native state. This conformation is also different from those of cytochrome *c* in the pH-denatured and molten globule states in solution.

This work was supported by a JSPS research grant for the Future Program, a grant on Priority Area of "Chemical Reaction Dynamics in Condensed Phases" (10206207), a Grant-in-Aid for Scientific Research (B) (13555015) from the Ministry of Education, Science, Sports, and Culture. This work was also supported by the Joint Studies Program (1998–2000) of the Institute for Molecular Science. We thank Prof. Teizo Kitagawa of the Institute for Molecular Science for allowing us to use his Raman spectrometer. We appreciate Prof. Shinji Saito of Nagoya University and Prof. Shoji Takada of Kobe University for helpful discussions.

References

1 X.-C. Zhang, B. B. Hu, J. T. Darrow, and D. H. Auston, *Appl. Phys. Lett*, **56**, 1011 (1990).
2 X.-C. Zhang and D. H. Auston, *J. Appl. Phys.*, **71**, 326 (1992).
3 N. Sarukura, H. Ohtake, S. Izumida, and Z. Liu, *J. Appl. Phys.*, **84**, 654 (1998).
4 H. Ohtake, S. Ono, M. Sakai, Z. Liu, T. Tsukamoto, and N. Sarukura, *Appl. Phys. Lett.*, **76,** 1398 (2000).
5 H. Harde, S. Keiding, and D. Grischkowsky, *Phys. Rev. Lett.*, **66**, 1834 (1991).
6 H. Harde and D. Grischkowsky, *J. Opt. Soc. Am. B*, **8**, 1642 (1991).
7 L. Thrane, R. H. Jacobsen, P. U. Jepsen, and S. R. Keiding, *Chem. Phys. Lett*, **240**, 330 (1995).
8 C. Ronne, L. Thrane, P. Astrand, A. Wallqvist, K. V. Mikkelsen, and S. R. Keiding, *J. Chem. Phys.*, **107**, 5319 (1997).
9 C. Ronne, P. Astrand, and S. Keiding, *Phys. Rev. Lett.*, **82**, 2888 (1999).
10 J. T. Kindt and C. A. Schmuttenmaer, *J. Chem. Phys.*, **100**, 10373 (1996).
11 D. S. Venables and C. A. Schmuttenmaer, *J. Chem. Phys.*, **108,** 4935 (1998).
12 D. S. Venables, A. Chiu, and C. A. Schmuttenmaer, *J. Chem. Phys.*, **113**, 3243 (2000).
13 D. S. Venables and C. A. Schmuttenmaer, *J. Chem. Phys.*, **113**, 11222 (2000).
14 M. C. Beard, G. M. Turner, and C. A. Schmuttenmaer, *J. Am. Chem. Soc.*, **122**, 11541 (2000).
15 G. Haran, W.-D. Sun, K. Wynne, and R. M. Hochstrasser, *Chem. Phys. Lett*, **274**, 365 (1997).
16 R. McElroy and K. Wynne, *Phys. Rev. Lett*, **79**, 3078 (1997).
17 A. G. Markelz, A. Roitberg, and E. J. Heilweil, *Chem. Phys. Lett*, **320**, 42 (2000).
18 K. Tominaga, H. Ohtake, N. Sarukura, K. Saitow, H. Sasakawa, A. Tamura, I. V. Rubtsov, and K. Yoshihara, *Adv. Multiphoton Processes Spectrosc.*, **13**, 317 (2001).
19 M. Brucherseifer, M. Nagel, P. H. Boliver, H. Kurz, A. Bosserhoff, and R. Buttner, *Appl. Phys. Lett.*, **77**, 4049 (2000).
20 Y. Seno and N. Go, *J. Mol. Biol.*, **216**, 111 (1990).
21 S. Hayward, A. Kitao, H. Hirata, and N. Go, *J. Mol. Biol.*, **234**, 1207 (1993).
22 S. Hayward and N. Go, *Annu. Rev. Phys. Chem.*, **46**, 223

(1995).
23 A. Kitao and N. Go, *Curr. Opin. Struct. Biol.*, **9**, 164 (1999).
24 H. J. Berendsen and S. Hayward, *Curr. Opin. Struct. Biol.*, **10**, 165 (2000).
25 N. Go, T. Noguchi, and T. Nishikawa, *Proc. Natl. Acad. Sci. U. S. A*, **80**, 3696 (1983).
26 K. G. Brown, S. C. Erfurth, E. W. Small, and W. L. Peticolas, *Proc. Nat. Acad. Sci. U. S. A*, **69**, 1467 (1972).
27 L. Genzel, F. Keilmann, T. P. Martin, G. Winterling, Y. Yacoby, H. Frohlich, and M. W. Makinen, *Biopolymers*, **15**, 219 (1976).
28 J. C. Smith, *Quart. Rev. Biophys.*, **24**, 227 (1991).
29 W. Doster, S. Cusack, and W. Petry, *Phys. Rev. Lett.*, **65**, 1080 (1990).
30 M. Diehl, W. Doster, W. Petry, and H. Schober, *Biophys. J.*, **73**, 2726 (1997).
31 M. Ferrand, A. J. Dianoux, W. Petry, and G. Zaccai, *Proc. Natl. Acad. Sci. U. S. A*, **90**, 9668 (1993).
32 A. Paciaroni, A. R. Bizzarri, and S. Cannistraro, *J. Mol. Liquids*, **84**, 3 (2000).
33 B. Fanconi, *Biopolymers*, **12**, 2759 (1973).
34 W. J. Shotts and A. J. Sievers, *Chem. Phys. Lett.*, **21**, 586 (1973).
35 U. Buontempo, G. Careri, P. Fasella, and A. Ferraro, *Biopolymers*, **10**, 2377 (1971).
36 W. J. Shotts and A. J. Sievers, *Biopolymers*, **13**, 2593 (1974).
37 M. Ataka and S. Tanaka, *Biopolymers*, **18**, 507 (1979).
38 K. D. Moeller, G. P. Williams, S. Steinhauser, C. Hirschmugl, and J. C. Smith, *Biophys. J.*, **61**, 276 (1992).
39 S. L. Chuang, S. Schmitt-Rink, B. I. Greene, P. N. Saeta, and A. J. Levi, *Phys. Rev. Lett.*, **68**, 102 (1992).
40 S. Ono, T. Tsukamoto, E. Kawahata, T. Yano, H. Ohtake, and N. Sarukura, *Appl. Opt.*, **40**, 1369 (2001).
41 Y. Kuroda, S. Kidokoro, and A. Wada, *J. Mol. Biol.*, **223**, 1139 (1992).
42 S. Krimm and J. Bandekar, *Adv. Protein Chem.*, **38**, 181 (1986).
43 S. Krimm, "Peptides and Proteins," in "Biological Applications of Raman Spectroscopy," ed by T. G. Spiro, John Wiley & Sons, New York (1987), Vol. 1, pp. 1–45.
44 J. F. Rabolt, W. H. Moore, and S. Krimm, *Macromolecules*, **10**, 1065 (1977).
45 T. G. Spiro and X.-Y. Li, "Resonance Raman Spectroscopy of Metalloporphyrins," in "Biological Applications of Raman Spectroscopy," ed by T. G. Spiro, John Wiley & Sons, New York (1988), Vol. 3, pp. 1–37.
46 S. Hu, I. K. Morris, J. P. Singh, K. M. Smith, and T. G. Spiro, *J. Am. Chem. Soc.*, **115**, 12446 (1993).
47 T. Jordan, J. C. Eads, and T. G. Spiro, *Protein Sci.*, **4**, 716 (1995).
48 S. Takahashi, S.-R. Yeh, T. K. Das, C.-K. Chan, D. S. Gottfried, and D. L. Rousseau, *Nature Struct. Biol.*, **4**, 44 (1997).
49 S.-R. Yeh, S. Han, and D. L. Rousseau, *Acc. Chem. Res.*, **31**, 727 (1998).
50 B. Cartring, "Cytochrome *c*," in "Biological Applications of Raman Spectroscopy," ed by T. G. Spiro, John Wiley & Sons, New York (1988), Vol. 3, pp. 217–248.
51 B. E. Bowler, A. Dong, and W. S. Caughey, *Biochemistry*, **33**, 2402 (1994).
52 M. L. E.-Fonberg, L. M. S. Worsham, and S. G. Williams, *Biochim. Biophys. Acta*, **1164**, 273 (1993).
53 F. M. Wasacz, J. M. Olinger, and R. J. Jakobsen, *Biochemistry*, **26**, 1464 (1987).
54 E. Bramanti, E. Benedetti, C. Nicolini, T. Berzina, V. Erokhin, A. D'Alessio, and E. Benedetti, *Biopolymers*, **42**, 227 (1997).
55 S. Y. Venyaminov and N. N. Kalnin, *Biopolymers*, **30**, 1243 (1990).
56 S. Y. Venyaminov and N. N. Kalnin, *Biopolymers*, **30**, 1259 (1990).
57 R. G. Gordon, Adv. Magn. Reson., **3**, 1 (1968).
58 D. A. McQuarrie, "Statistical Mechanics," HarperCollins, New York (1976).
59 B. J. Berne, "Time-dependent properties of condensed media," in "Physical Chemistry, an advanced treatise," ed by D. Henderson, Academic Press, New York (1971), Vol. 8B, pp. 539–716.
60 R. Shuker and R. W. Gammon, *Phys. Rev. Lett*, **25**, 222 (1970).
61 F. L. Galeener and P. N. Sen, *Phys. Rev. B*, **17**, 1928 (1978).
62 G. W. Bushnell, G. V. Louie, and G. D. Brayer, *J. Mol. Biol.*, **214**, 585 (1990).